2022-01-0440 Published 29 Mar 2022

Delamination Failure on High-Output Diesel Engine Thermal Barrier Coatings

Georgios Koutsakis University of Wisconsin Madison

John Saputo Stony Brook University

Eric Gingrich and Michael Tess US Army GVSC

Sanjay Sampath Stony Brook University

Jaal B. Ghandhi University of Wisconsin Madison

Citation: Koutsakis, G., Saputo, J., Gingrich, E., Tess, M. et al., "Delamination Failure on High-Output Diesel Engine Thermal Barrier Coatings," SAE Technical Paper 2022-01-0440, 2022, doi:10.4271/2022-01-0440.

Received: 25 Jan 2022 Revised: 25 Jan 2022 Accepted: 09 Jan 2022

Abstract

An analytical mechanics model was employed to predict the delamination of several thermal-barrier-coated pistons that had been previously tested in a high-output, single-cylinder diesel engine. Some of the coatings delaminated during engine operation. Results are presented for two thicknesses of the same coating material, and for two similar coatings with different levels of stiffness. All the coating thermomechanical properties such as thermal conductivity, density, volumetric heat capacity, thickness, elastic modulus, coefficient of thermal expansion, Poisson ratio and toughness, were measured prior to engine testing. Previous measurements of the piston transient heat flux, based on fast-response surface temperature data, in the same engine were used as an input to calculate the multilayer wall temperature distribution. A theoretical methodology was employed to evaluate and predict the coating durability. The method considers the release rate of elastic strain energy stored in the coating when it cracks as the main driving force for delamination; when the calculated energy release rate overcomes the toughness, coating crack failure is predicted to occur. The mechanics durability model was found to provide good trendwise comparison with the post-run coating integrity observations. When the energy release rate significantly exceeded the toughness, failure was indeed observed. Borderline cases, where the energy release rate was close to the material toughness, however, were more difficult to predict.

Introduction

Thermal barrier coatings (TBCs) have been pursued with mixed results as a pathway for increased efficiency in high output diesel engines for nearly half a century [1-9]. In this application durability issues and inconsistent performance benefits have been persistently reported in the literature. These issues have greatly limited the successful implementation of TBCs [10-12, 3, 13-15].

The coatings in this application have typically been derivatives of the thermal barrier coatings utilized in the aerospace industry — a low thermal conductivity ceramic 7-8 wt.% Yttria Stabilized Zirconia (YSZ) insulation layer applied over a nickel or cobalt based alloy "bond coat" layer that aids in adhesion of the ceramic and prevents oxidation of the base component. Significant advancements in processing science have resulted in extremely reliable coatings that are present in nearly all gas turbines, with a low likeliness for process-induced failures. Design-related failures, however, remain a significant challenge for such coatings.

In reciprocating engines, these challenges are magnified by the complex, highly transient thermal and mechanical environment caused by the combustion process. Some of the earliest work in this area attempted to use coatings with millimeter scale thickness [1, 11, 4-6, 9] and were plagued by cracking and delamination of the ceramic topcoat. This led to the use of functionally graded materials (FGMs), which were thought to reduce stresses by a continuous grading of the thermomechanical properties of the coating. While this has been successful for increasing the durability of thick coatings [9, 16], contemporary trends in coating design have evolved and present different requirements.

The use of thin coatings to reduce the volumetric efficiency penalties of thick coatings emerged as a design pathway in the late 1980s [17, 18]. While limited investigations were

performed using these "thin" TBCs over the following two decades [19-23], failures were reported far less often. Inadvertently, reducing coating thicknesses to the scale of hundreds of microns led to increased durability by reducing thermal stresses in the coating. Practically, this expanded the design space of permissible materials and allowed the use of lower toughness but more thermally beneficial ceramics. However, alternative TBC designs were not highly pursued at the time, with most investigations centered on YSZ-based coatings, where durability issues had been partially alleviated.

In the last decade reports of performance benefits from thin coatings of alterative materials [24, 25] have renewed interest in this pathway and advanced heat transfer techniques were developed to assess engine performance. The analytical solution development of unsteady heat conduction in multi-layer engine walls [26] enabled paramount computational efficiencies while guaranteed the accuracy. Conventional finite difference approaches were outperformed since this method only computes the output of interest [27-29]. The surface temperature is the only output of interest explicitly for providing boundary conditions to engine simulation. The technique was experimentally validated under steady-state engine operation [30] and full transient drive cycles [31]. A large-scale optimization was employed to identify the trade-off between engine performance and coating durability [32].

Furthermore, contemporary investigations have pursued a variety of different coating architectures and materials including thermal swing coatings produced from relatively thin low thermal conductivity and low volumetric heat capacity systems [24, 25, 33-35], specialized highly porous coatings materials [36, 14, 37, 38, 13, 39], and multilayer composites [34, 13, 39]. In many of these scenarios coating durability has again become a significant issue. However, the strategies used to increase the durability of thick coatings are not directly transferrable. A deeper understanding of the mechanics of coating delamination is required for successful coating design.

This study employs an analytical mechanics method to evaluate coatings' durability due to thermomechanical loading. A brief introduction of the proposed durability mechanics technique is described below while further details can be found in Koutsakis et al.[40].

The release of elastic strain energy stored in the coating, which builds up due to thermal stresses, supplies the main driving force for delamination in thermal barrier coating systems. The method requires the full multilayer wall temperature distribution during an engine cycle for calculation, and depends on mechanical properties such as elastic modulus, coefficient of thermal expansion and Poisson ratio. Figure 1 shows a thin thermal barrier coating bonded to a piston substrate. The left surface is exposed to the combustion gases while the right is oil-cooled. The combustion chamber surface temperature may vary anywhere between the intake stroke and combustion extremes, resulting in a wide temperature distribution envelope throughout the engine cycle. The approach taken is to assume that a crack exists at a specific location in the structure, see Fig. 1. The difference in strain energy, U, between the intact structure and the two parts separated by the crack is calculated and termed the elastic energy release rate, G

FIGURE 1 Schematic illustration of a thermal barrier coated steel wall exposed to combustion chamber gases (left) and coolant/oil (right). The wall temperature distribution is illustrated at various different times, *i.e.* intake, combustion and mid-expansion time during the engine cycle. A delamination due to crack propagation is illustrated near the mid-coating region.

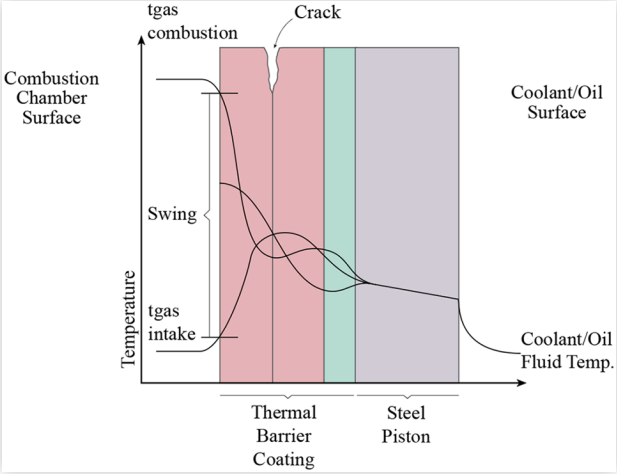

$$G = U^{\text{whole}} - \left(U^{\text{top}} + U^{\text{bottom}}\right) \tag{1}$$

where U^{whole}, U^{bottom}, and U^{top} are the strain energy of the intact multilayer, piston substrate, and debonded coating, respectively. The general methodology to calculate the energy release rate and the equations that estimate each strain energy, which are involved and can not be easily summarized, are given in Koutsakis et al. [40]. The hypothesis is that the crack will advance when G exceeds a threshold that depends only on thermomechanical material properties. The critical parameter is the toughness G_c of the material or the interface. The toughness is an experimental measurement, not a calculated parameter, and the measurements are described above. The calculated elastic energy release rate, G, with units of energy/area is a function of specimen geometry, material properties and thermomechanical load. Crack growth is initiated when the energy release rate overcomes toughness, as given in Eq. (2).

$$G \geq G_c \tag{2}$$

Experimental Setup

Single-Cylinder Research Engine

Engine experiments were conducted on a single-cylinder research engine designed for high-output diesel operation. Full details of the engine laboratory can be found in Gingrich et al. [41]. A brief summary of the engine is provided here with engine specifications given in Table 1. Air was provided by an

TABLE 1 Single-cylinder research engine specifications

Displacement volume	1.49 L
Stroke	128 mm
Bore	122 mm
Connecting Rod	239 mm
Compression Ratio	14.0:1
Number of valves	4
Swirl ratio	1.3
Peak firing pressure	250 bar

external compressed air system that dries the air to a dew point less than -40°C. The intake air was temperature- and flow-controlled to simulate a turbocharger for steady-state measurement points. Exhaust back pressure was controlled via ball valves in the exhaust system. Air was delivered using a control valve, with feedback from a Coriolis flow meter plumbed in series. A high-pressure common rail fuel system was used to deliver fuel to the combustion chamber at pressures up to 2000 bar. A Bosch CRIN3 injector with an 8×167 μm hydro-ground nozzle (147° included angle) was used. All experiments were run with an AC dynamometer absorbing load and maintaining speed control of the engine.

Single-cylinder engine experiments were run over five different operating conditions shown in Table 2. For each operating condition a start of injection (SOI) sweep was conducted. The injection duration was held constant, which meant load varied slightly with changes to SOI. In most cases, the earliest injection timing was limited by excessive peak in-cylinder pressure, and the latest injection timing was limited by either excessive exhaust temperature or exhaust smoke.

The conditions were primarily selected to explore the performance and heat rejection benefits of thermal barrier coatings at high-load engine operation. Additional details of each operating condition can be found in Gingrich et al. [42]. This work will not discuss engine performance; it utilizes the cumulative engine run time and thermal loading to explore coating durability. Additionally, the piston heat flux has been extensively measured for these conditions, discussed in the following section, and these measurements served as an input to the analytical mechanics method to predict coating delamination.

Piston Heat Flux

Piston heat flux data, summarized here, were acquired on an uncoated steel piston for engine operating conditions 1-5 in a previous study [41]. A thermocouple-instrumented piston

FIGURE 2 Location of 15 fast-response thermocouples on the metal piston in reference to other engine features

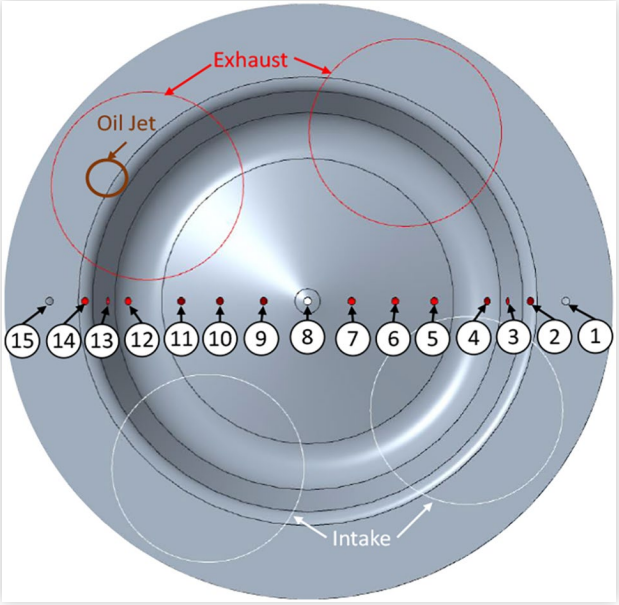

with a wireless telemetry system was used to record the high-speed piston surface temperature. Figure 2 shows the position of 15 fast-response thermocouples flush-mounted in the piston crown. The thermocouples were installed in a plane perpendicular to the piston wrist pin with roughly equal spacing along the piston diameter.

The time-resolved temperature data at each location were used to calculate heat flux to the metal wall. Assuming a semi-infinite wall with periodic boundary conditions, the solution is in the form of a Fourier series, and therefore a fast Fourier transform (FFT) can be used to decompose the surface temperature data and reconstruct the heat flux That is not the case for multilayer engine walls. The FFT method, as it is commonly known, has been widely used to calculate surface heat flux in internal combustion engines [43, 44].

The FFT solution is a two-part solution with a steady state and transient portion. The transient portion of the solution only requires the instantaneous surface temperature, whereas the steady-state term requires a second, steady-state temperature, at a known distance below the first. The thermocouples used to calculate heat flux did not include a backside temperature measurement, so only the transient solution could be calculated. An *ad hoc* method was used to recover the steady-state portion of area-averaged heat flux based on the mean piston temperature and instantaneous gas temperature crossover point during the cycle. The resulting area average

TABLE 2 Summary of engine operating conditions

Condition	Speed [rpm]	IMEPg [bar]	AFR [-]	Fuel Pressure [bar]	Duration [°]
1	1700	12.3	29	1200	10.7
2	1500	23.8	24.5	1700	18.6
3	2500	20.3	26.8	2000	21.6
4	1700	30.3	24.5	2000	25.0
5	2750	29.7	25.5	2000	40.5

FIGURE 3 Operating condition 3 (2500 rpm, 20.3 bar IMEPg) SOI timing of -29°aTDC (a) area-averaged and individual heat flux with line color indicating piston location and (b) contour of heat flux integrated with time (energy flux) from -20 to 100°aTDC, adapted from Gingrich [45].

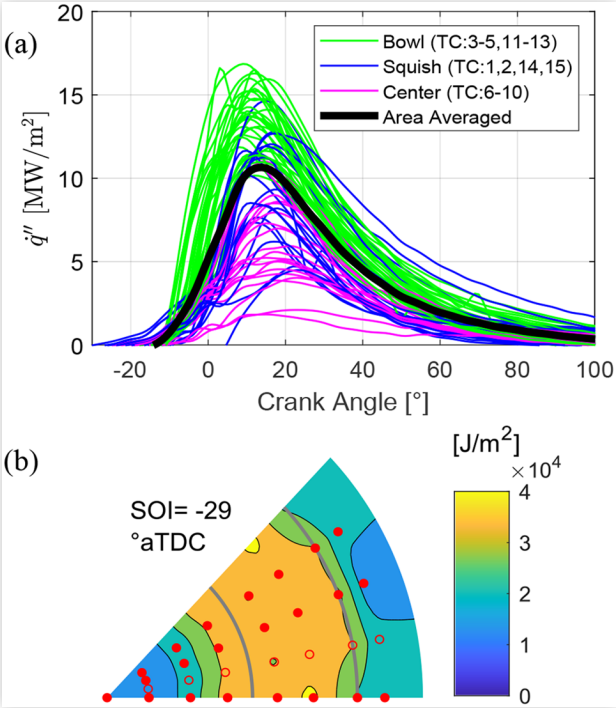

heat transfer was then compared to other independent measurements of engine heat transfer, which showed good agreement across all operating conditions. For details on heat flux calculation and validation see Gingrich et al [41].

Figure 3 (a) shows the average and individual location heat flux data grouped by piston location for operating condition 3 (2500 rpm, 20.3 bar gross Indicated Mean Effective Pressure (IMEPg)), injection timing of -29° after Top Dead Center (aTDC). The highest heat flux was observed in the piston bowl area. Lower heat flux was observed toward the center of the piston and in the squish region (outer diameter). The area-average heat flux shown in Fig. 3 (a) only includes the transient solution, which will later shift slightly upward once the steady-state solution is recovered. The larger variation of heat flux in the squish is believed to be related to spray plume variation which is expected to be larger in the squish. Regions of hot gas (on-plume) are likely more separated by cooler gas as the sprays travel radially outward. The "Squish" region nomenclature includes piston bowl lip thermocouples, which is a transition region for spray plumes as they move radially outward and would likely be more sensitive to small variations in spray targeting. Figure 3 (b) shows the spatial distribution of heat fluxes integrated with respect to time (energy flux) from -20 to 100°aTDC. The analytical mechanics method to predict coating delamination presented in this paper utilized the average heat flux, including the steady-state solution, scaled by a factor of 1.5, as shown in Fig. 4. The scaled heat flux corresponds to the maximum expected heat flux in the piston bowl region and is considered a better

FIGURE 4 Estimated local bowl-wall and global area-weighted heat fluxes obtained via telemetry measurements on an uncoated piston, including the steady-state solution.

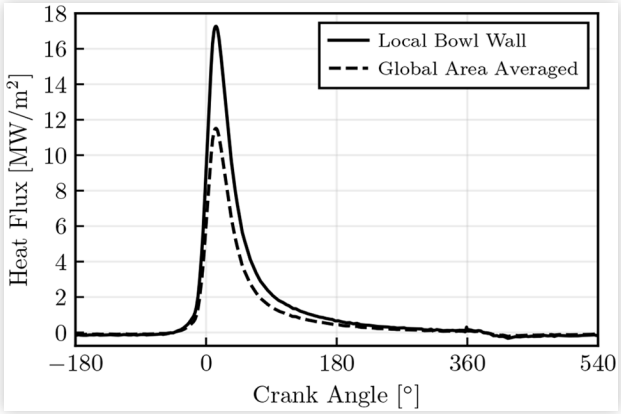

representation than selecting a single location's value from Fig. 3 (a). The scale factor of 1.5 is derived from the approximate ratio of peak local heat flux to peak average heat flux in Fig. 3 (a).

Operating condition 3 at an injection timing of -29°aTDC was found to have the highest heat flux among all the conditions investigated in the uncoated metal piston testing [45], which is why it was selected and utilized in this paper as the worst case scenario to analyze for a possible coating delamination failure. Global heat transfer estimations based on measurements of fluid enthalpy and work did not indicate a significant change to heat transfer for any of the coated pistons, and therefore utilizing the metal piston heat flux as an estimate for the heat flux on a coated piston is reasonable. Overall, utilizing the highest heat flux operating condition from the uncoated telemetry experiments, scaled based on spatial gradients, should be representative of the maximum heat flux experienced on the piston during all testing.

Thermal Barrier Coatings

Collaboration between the Center for Thermal Spray Research and the U.S. Army Ground Vehicle System Center has resulted in a unique opportunity to explore the factors governing coating delamination in diesel engines. More than 20 coated pistons have been produced, extensively characterized, and tested in a single-cylinder research engine. Of these, three scenarios are explored here in depth. The first is a traditional YSZ-based thermal barrier coating system of two thicknesses, the second a novel low-thermal conductivity and low-volumetric heat capacity coating with two variations in compliance, and the third is a functionally graded type with performance benefits previously detailed [42]. While many more coated systems were investigated in this collaborative effort, these cases were selected as being representative of both traditional and contemporary coating designs.

Table 3 gives the details of each of the coatings and defines the nomenclature. All of the coatings except "YSZ Thick", were run for varying times at engine operating conditions 1-5.

TABLE 3 Summary of engine operating conditions

Internal Nomenclature	Wall Structure	TBC Material	Total TBC thickness [μm]	Functionally Graded	Conditions Run	Hours Run	Delamination
TBC3 Build5	Four-layer YSZ [42]	YSZ	325	Yes	1-5	75	No
TBC11 Build20	Thin	YSZ	325	No	1-5	26	No
TBC13 Build26	Thick	YSZ	474	No	3, 5	4	Yes, at bowl wall
TBC8 Build15	Compliant	Cordierite-YSZ	350	Yes	1-5	40	No
TBC16 Build 35	Stiff	Cordierite-YSZ	351	Yes	1-5	40	Yes, at bowl wall

For "YSZ Thick", delamination was observed upon completion of a 4 hours break-in schedule, which consisted of progressively increasing load/speed and culminating in the two high load points (conditions 3 and 5). The total testing time for the other cases ranged from 26-75 hours and was primarily focused on performance testing. The "Cordierite-YSZ Stiff" also experienced a delamination that was not observed until after testing was complete, so the exact time delamination occurred is unknown. Both coating delaminations occurred in the piston bowl area. Images of the "YSZ Thick" and "Cordierite-YSZ Stiff" can be found in Fig. 8 and 11, respectively.

Materials Fabrication

An argon-hydrogen atmospheric plasma spray (APS) process (F4MB, Oerlikon Metco, Westbury, NY, USA) configured with a 6 mm nozzle and a 90° 1.8 mm injector was used to fabricate coatings on piston crowns and for thermal and mechanical property measurement. Before deposition all surfaces were degreased, and grit blasted at 80 psi from a 125 mm distance using 24 mesh alumina grit. Primary and secondary gas flow rates, arc current, and carrier gas flow rates for each coating are listed in Table 4 in the Appendix. Carrier gas flow rates were optimized on a per-run basis, as described elsewhere [46], to ensure the development of consistent coatings between experiments. Finally, during the spray process, the surface temperatures were monitored using a long wave infrared imaging system (A655SC, FLIR Systems, Wilsonville, OR, USA) to estimate each coating's stress-free temperature.

Four material variations were produced: a composite NiCr-Al bond coat (443NS, Oerlikon-Metco, Westbury, NY, USA), an 8 wt% Yttria-Stabilized Zirconia TBC (SG204, St. Gobain Coating), and two variations of a Cordierite-YSZ glass-ceramic composite based on previous work [33]. The first cordierite-YSZ composite (Cordierite-YSZ Compliant) was produced from a coarse spray-dried cordierite feedstock (Superior Technical Ceramics, St. Albans, VT, USA) blended with YSZ feedstock fifty percent by volume before spraying. The latter (Cordierite-YSZ Stiff) was produced with a fine fused powder (Oerlikon-Metco, Westbury, NY, USA) similarly blended before spraying.

Coatings for thermal and mechanical property measurements were deposited on the face of 12.7 mm diameter graphite rods and 27 × 127 × 13 mm graphite plates by moving the torch normal to the surface in a raster pattern at a constant 250 mm/s velocity. After deposition coatings were ground into freestanding forms using silicon carbide emery paper and machined into 12.5 × 0.75 mm disks and 5 × 2.5 × 25.4 mm bars. The former were used in the measurement of thermal diffusivity, density, and specific heat, while the latter were used to assess the coatings elastic modulus, coefficient of thermal expansion, and the critical stress intensity factor for fracture, which is used to derive toughness.

Following property evaluation, the coatings were deposited on piston crowns by traversing the torch across the crown geometry while rotating the piston. The torch was kept normal to the surface and a 250 mm/s surface speed maintained by varying the linear velocity of the torch. Further air cooling was utilized to maintain a uniform deposition temperature, which was monitored using the infrared imaging system described earlier. To ensure coating uniformity across the component geometry mock parts were coated, cross sectioned, and inspected. Information gathered from cross sections was then used to iteratively improve the torch tool-path and generate uniform coatings.

Thermal Property Measurements

Thermal diffusivity and specific heat were simultaneously measured using a standardized thermal flash method (Discovery Xenon Flash DXF 900, TA Instruments, New Castle, DE, USA), while density was measured using Archimedes principle and a precision mass balance. Diffusivity was calculated using corrections for convective heat losses and a finite pulse width per ASTM E1461 [47] standards, and the product of diffusivity, density, and specific heat were used to calculate thermal conductivity. Finally, the secant coefficient of thermal expansion (CTE) was evaluated between 100 and 800°C using an alumina pushrod dilatometer (DIL 402C, Netzsch, Selb, DE) using 15 cN of force.

Mechanical Property Measurements

APS ceramic coatings, including those characterized here, are often anisotropic and non-linear elastic solids due to their complex defect structures [48-51]. This generally results in their stiffness greatly decreasing with applied tensile strain [48] and properties varying by as much as a factor of two in the through-thickness and in-plane directions [52]. Additionally, in an ambient environment, APS coatings have a complex neutral stress state (residual stress) that varies though the thickness and can further complicate analysis [53, 54]. While ignoring these effects may be expected to cause a significant overestimation of energy release rates, simplification of the coating's mechanical behavior can be made to

employ the analytical mechanics method, developed in Koutsakis et al. [40], to provide insights into observed failures during engine tests.

Generally, the coatings are assumed to be isotropic and linear-elastic, and the elastic modulus E and Poisson ratio ν were evaluated at small strains using an impulse excitation technique (SA-BP, Sonelastic Division, ATCP Physical Engineering, Riberirao Preto, Brazil). The flexural vibrational frequency was measured and used to calculate flexural modulus as described elsewhere [55-57].

While critical stress intensity factors can vary as described above, similar assumptions were made to assess the coatings' fracture behavior. Critical stress intensity factors were measured in a single edge notch bend (SENB) configuration following ASTM E1820 [58] standards, and the critical energy release rate was estimated as only the elastic contribution of energy release rate as:

$$G_c \simeq \frac{K_{IC}^2\left(1-\nu^2\right)}{E} \tag{3}$$

where G_c is toughness in [kJm^{-2}], K_{IC} is fracture toughness or critical stress intensity factor in [MPa $\sqrt{}$ m], ν is the Poisson ratio , and E is the Young's modulus in [GPa]. While more complex testing can be performed to directly measure the critical energy release rates, or inclusion of a plastic or non-linear elastic component could be pursued [59, 60], this formulation was chosen as the model.

In this test, three-point loading was performed on a universal testing machine (Model 26005, TIRA GmbH, Schalkau, Germany) with samples supported on rollers spaced 21 mm apart. Before testing, a notch is machined into the samples and a third roller is centered over this and used to bend the sample at a deflection rate of 0.06 mm/min, opening a crack in this location. The onset of cracking occurs at a load, P_c, after which the measured load begins to decrease. The critical stress intensity factor, K_{IC}, is calculated using P_c and the sample dimensions as outlined elsewhere [52]. Finally, the stress-free reference temperature was taken as the mean surface temperature measured during coating deposition. All the material properties discussed above are outlined in Table 5 found in the Appendix.

Durability Mechanics Approach

Four-Layer YSZ Wall Architecture

In this section, the engine performance and mechanics characteristics are demonstrated for the four-layer YSZ [42] coating deposited on the steel piston substrate, see Table 5. Figures 5 (a) and (b) show the gas cylinder pressure, gas cylinder temperature, apparent chemical heat release rate (AHRR), and the estimated local bowl-wall heat flux as a function of crank angle from engine experiments at operating

FIGURE 5 Temporal evolution, for the Four-layer YSZ wall architecture, (a) of gas pressure and gas temperature, (b) apparent chemical heat release rate and combustion chamber heat flux, (c) wall temperature distribution, (d) *x*-direction stress distribution, and (e) elastic energy release rate distribution. Stress-free temperature was held constant at 220°C.

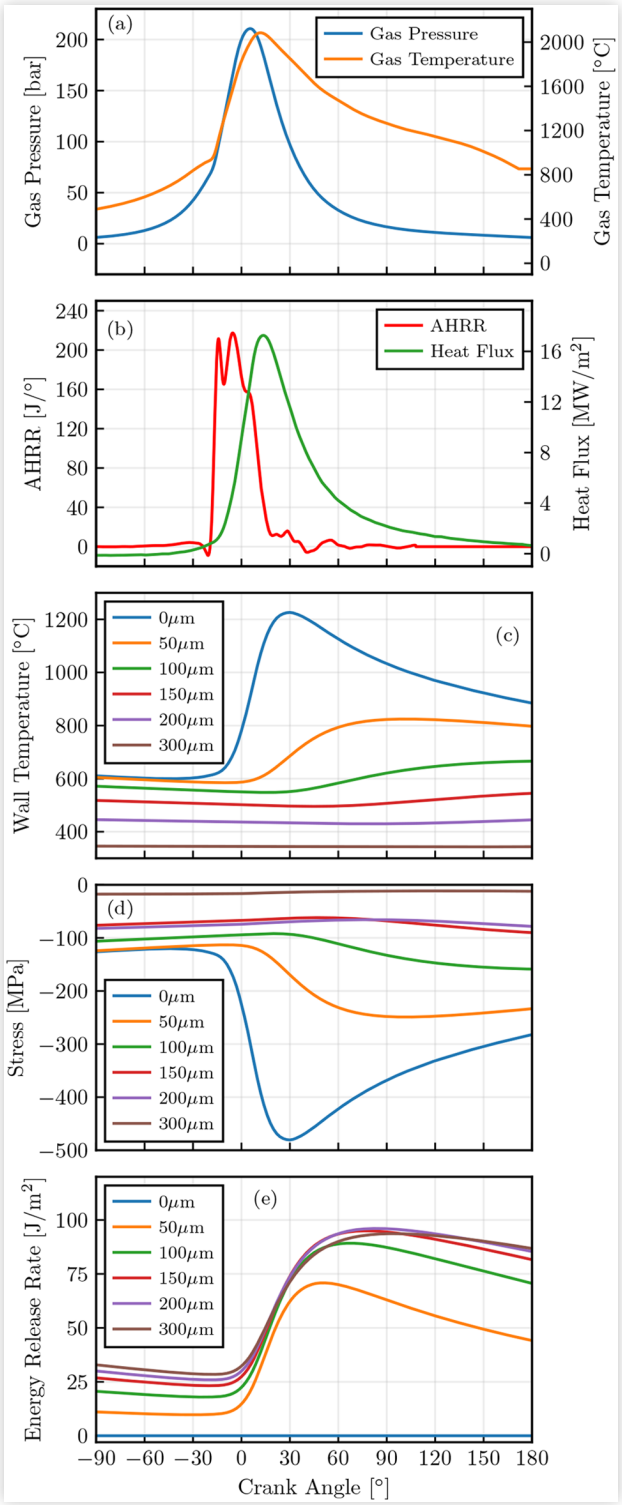

condition 3. The rated power condition gives peak pressure and temperature higher than 200 bar and 2000°C, respectively. A Crank-Nicolson finite difference scheme [27, 29] was employed to solve the 1-D heat conduction equation and generate the wall temperature distribution. The oil temperature on the backside remained fix at 100°C. The wall temperature histories of six discrete y-locations in the wall, where 0 is the combustion surface, are shown in Fig. 5 (c).

The x-direction stress histories, in the plane parallel to the piston surface, at the same y-positions are shown in Fig. 5 (d). Negative and positive values indicate compressive and tensile stress, respectively. It is worth noting that the vast majority of a thermal barrier coating system is under compression, even at ambient temperature. During the plasma deposition cooldown process, the ceramic molten particles cause the surface to tension and, by reaction, the multilayer wall compresses. the As heat flux and surface temperature increase due to combustion, the compressive stresses in the coating increase. The stress change at the interface is attributed more to static deformation due to changes in the coefficients of thermal expansion between materials than temperature changes.

Energy release rate histories for the same y-positions are illustrated in Fig. 5 (e). The energy release rate is zero at the surface by definition. Figure 6, however, provides a more comprehensive view of the energy release rate distribution through the coated engine wall. The temporal and spatial evolution of the temperature (a), x-direction stress (b), and energy release rate (c) are shown for the same engine condition as Fig. 5. The horizontal and vertical axes represent crank-angle (or time) and position in the wall, respectively. The latter has four different linear scales, which correspond to the thicknesses of the various layers of the as-sprayed multilayer coating: 0-195 μm, which is the top layer, 195-260 μm which is the gradient layer, 260-325 μm which is the bond layer and 325-5000 μm which is the piston substrate. The top-gradient, gradient-bond and bond-substrate interfaces are shown with horizontal pink lines. A typical coated engine wall temperature distribution is shown in Fig. 6 (a). The YSZ coating reaches a maximum temperature on the surface at 30°aTDC, slightly delayed relative to the maximum cylinder gas pressure and gas temperature, which occur at 5.5°aTDC and 12°aTDC, respectively, as shown in Fig. 5 (a). The temperature swing rapidly diminishes while the thermal wave progresses deeper into the wall; the interfaces (pink) have temperature swings (starting from the combustion surface) of about 36, 7 and 4°C, respectively. The intra-cycle wall temperature variations in the piston substrate are negligible.

The thermal shock at the combustion chamber surface, starting from TDC, contracts the bottom of the substrate further as localized heating in the coating causes the top surface to elongate, inducing downward curvature [40]. In addition, the stress-free temperature is fixed at 220°C and is responsible for compressive stresses in the coating seen in Fig. 6 (b). The maximum stress in the wall is observed to be exactly when and where the temperature is maximized at the surface, *i.e.*, 30°aTDC.

The energy release rate is seen in Fig. 6 (c). By definition the energy release rate at the edges (combustion chamber and coolant surface) are zero since there is no strain released there. Immediately after the start of combustion the energy release rate increases rapidly throughout the coating multilayer, even

FIGURE 6 Spatial and temporal (in crank angle domain) evolution of (a) temperature, (b) stress and (c) energy release rate using the wall architecture "Four-layer YSZ". Combustion chamber surface and oil surface are at y = 0 and y = 5000 μm, respectively. The interfaces are indicated with the horizontal pink lines at 195, 260 and 325 μm. The stress-free temperature was 220°C. The yellow star highlights the location of the maximum energy release rate.

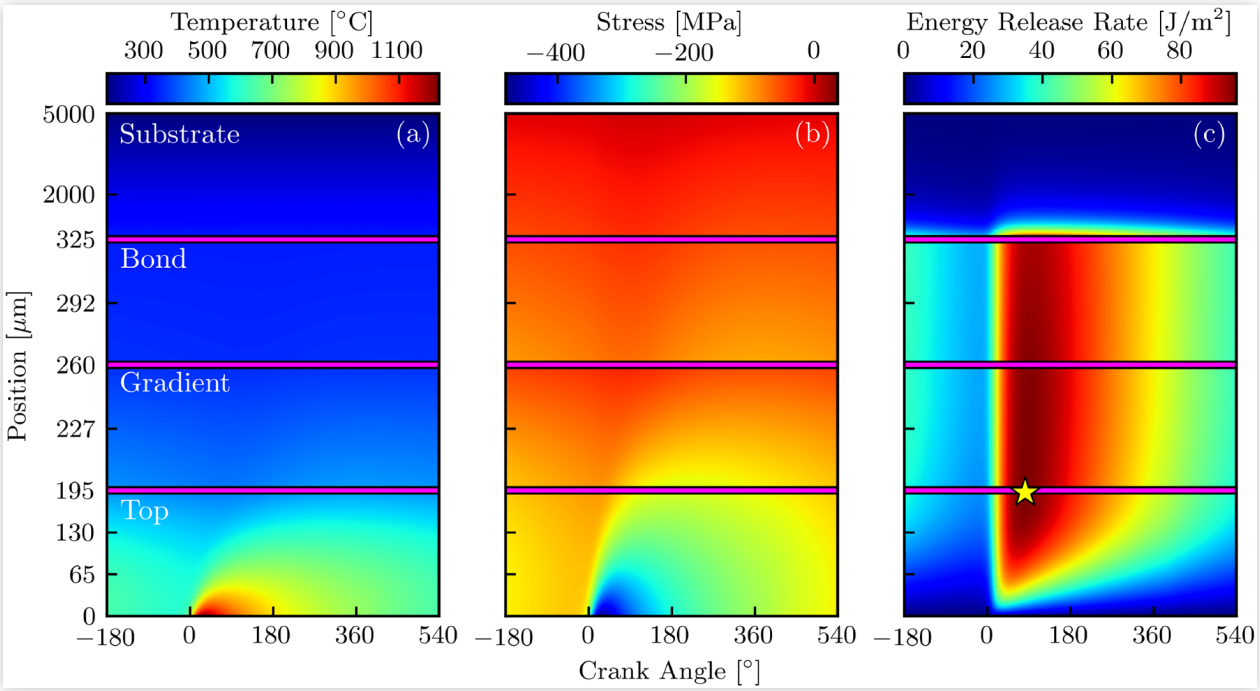

FIGURE 7 Energy release rate spatial distribution for coated region at three distinct crank angle locations is shown for the Four-layer YSZ architecture. The results shown are at TDC, 60°aTDC and BDC. The shaded areas highlight the top (orange), gradient (purple) and bond (green) coat thicknesses. The same engine condition as Fig. 5 and 6 was used.

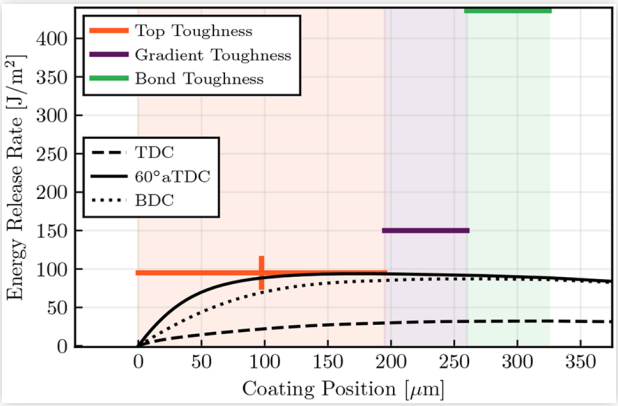

extending into the piston substrate. The maximum energy release rate is observed during the expansion stroke, at 82°aTDC at 192 μm (near the top-gradient interface) as highlighted with the yellow star. At this time of the cycle the coating surface is cooling while the interior of the coating is still heating. It is interesting to note that the position of the maximum energy release rate is near the mid-point of the top coat and is nearly constant through the gradient and bond coat. The surface layer has the lowest toughness and therefore controls the mechanics of this problem. This behavior suggests that, for cases where energy release rate exceeds the fracture toughness, the coating would have higher likelihood to crack at the top-gradient layer interface.

Figure 7 shows the spatial distribution of the energy release rate through the coating section (shaded area ranging from 0 to 325 μm). The combustion chamber gas and the piston substrate are to the left and right hand side of the shaded area, respectively. Energy release rate results are depicted for the crank angle times of TDC, 60°aTDC and BDC. It is evident that energy release rate is maximized near the mid-point of the top coat.

At TDC, the wall has only absorbed a small fraction of the total thermal energy and the temperature has not increased substantially. During the expansion stroke (60°aTDC), the energy release rate maximizes because the thermal wave has propagated through the coating and the surface temperature is decreasing from expansion cooling, as illustrated in Fig. 6 (a). At BDC, the thermal energy has penetrated most of the way through the coating.

The toughness of the top, gradient and bond layers are depicted in Fig. 7 with the horizontal orange, purple and green lines, respectively. The uncertainty given to the toughness measurements is provided with a 95% confidence interval, unless otherwise stated. The maximum energy release rate reaches almost the average top layer toughness, making it difficult to predict whether this structure would survive or fail. It is worth noting that the prediction is within the thermomechanical property uncertainties, indicated with the vertical orange error bar. Recall that in the lab experiments discussed above, the four-layer YSZ structure survived the testing schedule.

The Role of Coating Thickness

The role of coating thickness on the maximum energy release rate (in a cycle) was parametrically investigated in a previous study [40]. The coatings studied showed a non-linear increase of the maximum energy release rate with thickness, and a similar trend is observed for the YSZ thickness comparison described next. In the current work, a YSZ Thin (325 μm) and a YSZ Thick (520 μm) coating structure allowed the effect of thickness on the energy release rate to be tested. The key distinction between the four-layer YSZ and the two (thin and thick) YSZ is the absense of the gradient layer between the top and bond coat. The two cases matched all thermomechanical properties, but the (top layer) thickness differed by 2×, as shown in Table 5. The Thin version was operated across all engine conditions for a total of 26 hours and survived. However, the YSZ Thick version was observed to delaminate after the completion of an engine break-in test schedule, for which the last two test points were single SOIs at conditions 3 and 5. Post-run inspection showed that the coating was delaminated in the bowl wall area, as shown in Fig. 8. Looking at the top view of Fig. 8, one can observe the coating spalled at multiple locations. There are missing chips at every spray impingement location (near the central area of the soot witness mark), plus at some inter-plume regions. The coating first delaminates and then the delaminated region spalls off. As a side note, this observation further supports the argument that the highest piston heat fluxes are located *on* the spray axis, as shown in Fig. 3 [61, 45]. The durability analysis was employed to assess whether the analytical mechanics model could predict the observed coating failure.

Figure 9 shows the energy release rate distribution as a function of the wall position thru depth. The only crank-angle shown corresponds to the maximum energy release rate timing for each coating; the YSZ Thin and the YSZ Thick energy release rate distributions are shown at 87°aTDC and 106°aTDC, respectively. The vertical dashed blue and red lines indicate the coating-piston interface. Average toughness values are shown for the top and bond coating, respectively. The uncertainty from the average top layer toughness is depicted with the semi-transparent green rectangle, derived from 30 measurements on equivalent coupons.

The maximum energy release rate of YSZ Thin is *lower* than the toughness value, which is consistent with the engine testing where this coating survived. The maximum energy release rate for the YSZ Thick coating was *higher* than the toughness, indicating that such scenario could lead to coating failure, and this coating did fail in lab testing. The modeling results seem to capture the effect of thickness on the delamination crack-driving force and trendwise predict the coatings' mechanical performance.

FIGURE 8 Post-test piston images of the YSZ Thick

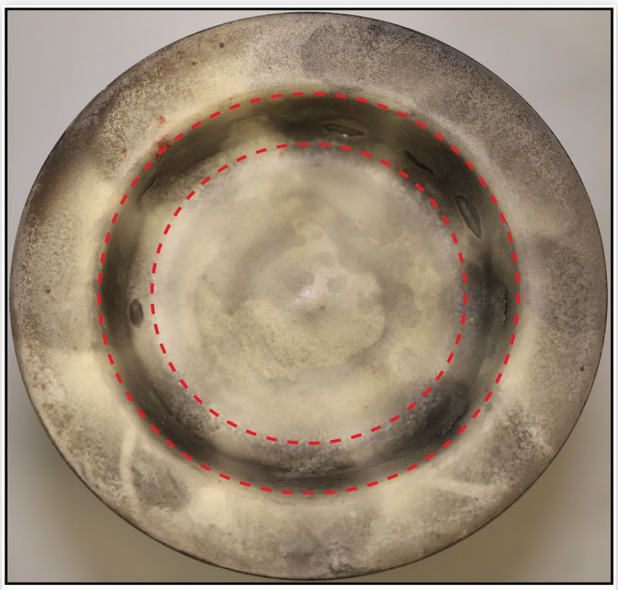

(a) Piston Top view

(b) View close to a delamination spot

FIGURE 9 Energy release rate spatial distribution is shown for the full wall depth. The distributions are shown for the maximum energy release rate crank-angle location of each case. The same YSZ coating is compared for two different thicknesses. The shaded area highlights the top layer toughness uncertainty.

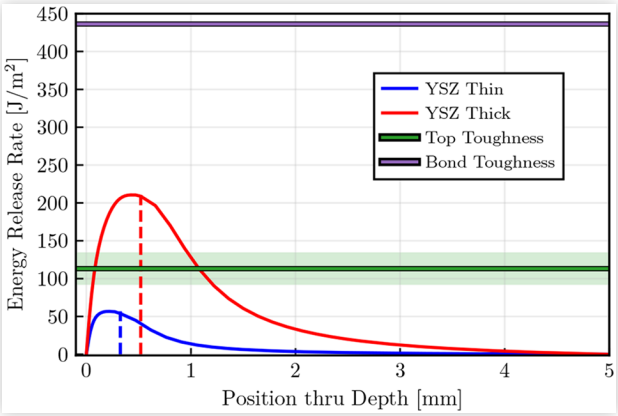

The Role of Coating Stiffness

The dependence of energy release rate on the coating modulus is strictly linear in the steady state isothermal cooling scenario of coated gas turbine blades [62]. Internal combustion engines undergo rapid transient thermal cycling, therefore the energy release rate could have a different dependence on the coating modulus.

A Compliant (15 GPa) and a Stiff (47 GPa) Cordierite-YSZ structure were fabricated to assess the effect of modulus on the energy release rate. The two versions reasonably matched all thermomechanical properties, but the Young's modulus of the Stiff was more than 3× the Compliant, as shown in Table 5. The thermal property matching, however, was not perfect. The stiffer version was achieved by depositing finer powder onto the piston substrate, which increased the density and thermal conductivity. Each version was tested across all engine conditions for total of 40 hours and inspected post-test. The Compliant coating survived the engine testing. The Stiff coating delaminated during testing.

Figure 10 shows the energy release rate distribution as a function of (a) total wall and (b) coating position. The dark grey and light grey shaded areas highlight the top and bond coat thickness, respectively. The only crank-angle shown corresponds to the maximum energy release rate distribution. The Compliant and the Stiff energy release rate distributions are shown at 85°aTDC and 76°aTDC, respectively. Each coating structure has its own toughness, unlike the thickness comparison scenario above. Horizontal lines depict the average top layer toughness for the Compliant (blue outlined with black) and the Stiff (red outlined with black) coatings. The uncertainty from the average top layer toughness of each material is shown with the trasparent rectangles, derived from 30 measurements on equivalent coupons.

The maximum energy release rate of the Compliant is *lower* than the average toughness, therefore the model captures correctly that this coating survives during engine testing. On the other hand, the maximum energy release rate of the Stiff is *nearly equal* to the average toughness making the prediction of whether this coating would delaminate difficult. Recall the Stiff coating failed during testing. By taking a closer look at the top view of the Stiff Cordierite-YSZ, see Fig. 11, one can clearly see that there are only a few delamination spots. By contrast, the YSZ Thick case showed signs of coating failure (coating and/or spalling) at every plume impingement location. The margin that the maximum energy release rate exceeded the toughness for the YSZ Thick case was substantial, see Fig. 9.The Stiff coating operated significantly close to its mechanical limits, but it did not overcome them to the same level as the YSZ Thick. Trendwise, therefore, the model is performing well.

Conclusions

The structural integrity of five thermal barrier coated pistons, having different coating properties, was modeled and compared to test results from a high-output, single-cylinder diesel engine. Two coating architectures delaminated during

FIGURE 10 Energy release rate spatial distribution is shown for (a) the entire engine wall and (b) the coating region. The distributions are shown for the maximum energy release rate crank-angle location of each case. The dark and light grey shaded area highlights top and bond coat thickness, respectively.

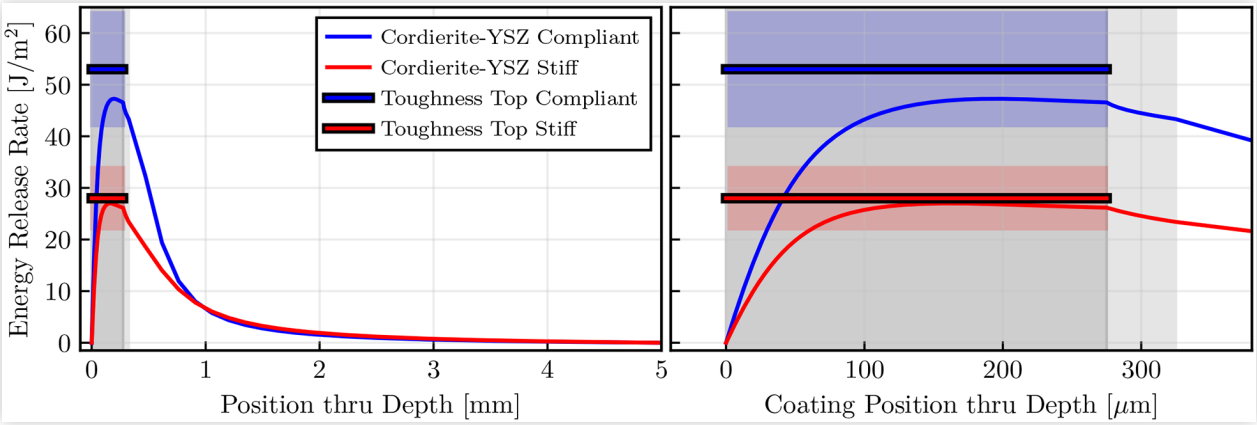

FIGURE 11 Post-test piston images of the Cordierite-YSZ Stiff

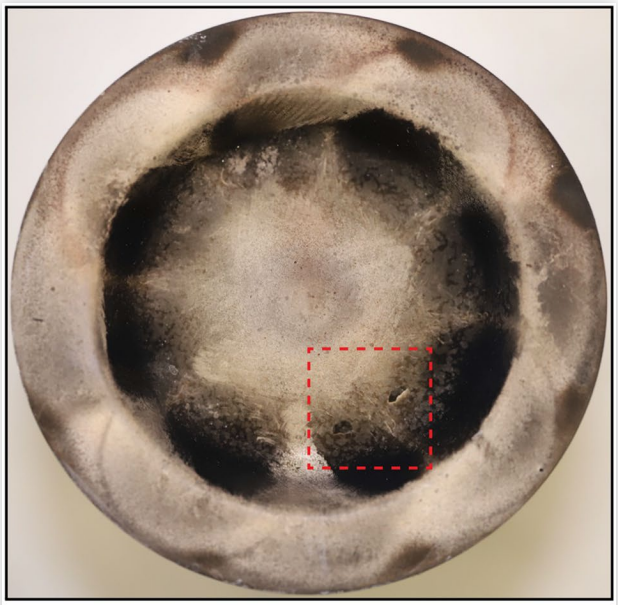

(a) Piston Top view

(b) View close to a delamination spot

engine operation. An analytical mechanics model was employed to predict the coating delamination.

Piston heat flux measurements from an earlier study on this engine used to estimate the highest heat flux observed in the bowl wall region. The local bowl-wall heat flux data served as an input to the mechanics method. The temperature distribution was predicted using a one dimensional finite difference method with boundary the time-varying heat flux and a fixed oil temperature applied to the combustion chamber surface and backside oil surface, respectively.

All coating thermomechanical properties were measured prior to engine testing. The property measurements included thermal conductivity, specific heat capacity, density, thickness, elastic modulus, coefficient of thermal expansion, Poisson ratio and critical stress intersity factor which led to toughness.

The mechanics model predicted a maximum energy release rate at locations near the center of the multilayer coating, not at the piston-coating interface. However, the spatial gradient was minor through the gradient and the bond coat layers. The maximum energy release rates also occured about midway down the expansion stroke when the combustion surface was cooling while the interior wall was still undergoing heating.

The on-engine coating durability observations and model results were consistent, within the uncertainty limits, for all five thermal barrier coatings. Coatings with maximum energy release rate that significantly exceeded the toughness failed; those with maximum energy release rate significantly below the material toughness survived. The thick YSZ case, which had significantly higher maximum energy release than its toughness, spalled on multiple locations along the bowl wall area plus some interstitial regions. The Stiff Cordierite-YSZ case, which had maximum energy release rate close to its toughness, spalled only on a couple locations along two spray plume axes, radially inward the deepest part of the bowl. Clear evidence of delamination was seen on both failed cases. The four-layer YSZ case, which had maximum energy release rate nearly equal to the toughness and within its uncertainty, however, showed no indication of durability issues. Therefore,

the model shows good trendwise predictive capability but caution should be used when assessing borderline cases.

References

1. Siegla, D.C. and Alkidas, A.C., "Evaluation of the Potential of a Low-Heat-Rejection Diesel Engine to Meet Future EPA Heavy-Duty Emission Standards," *SAE Transactions* 98 (1989): 294-302.
2. Assanis, D.N., Wiese, K., Schwarz, E., and Bryzik, W., "The Effects of Ceramic Coatings on Diesel Engine Performance and Exhaust Emissions," SAE Technical Paper 910460 1 (1991), doi:10.4271/910460.
3. Tricoire, A., Kjellman, B., Wigren, J., Vanvolsem, M. et al., "Insulated Piston Heads for Diesel Engines," *Journal of Thermal Spray Technology* 18, no. 2 (2009): 217-222.
4. Kamo, R., Bryzik, W., Reid, M., and Woods, M., "Coatings for Improving Engine Performance," *SAE Transactions* (1997): 354-363.
5. Siegla, D.C. and Amann, C.A., "Exploratory Study of the Low-Heat-Rejection Diesel for Passenger-Car Application," *SAE Transactions* (1984): 259-283.
6. Vittal, M., Borek, J., Marks, D., Boehman, A. et al., "The Effects of Thermal Barrier Coatings on Diesel Engine Emissions," *Journal of Engineering for Gas Turbines and Power* (1999).
7. Kvernes, I., Fartum, P., and Henriksen, R., "Development and Engine Testing of Coatings on Diesel Engine Components," *Central Inst. for Industrial Research, Oslo (Norway)* (1979).
8. Kamo, R., "Adiabatic Turbocompound Engine Performance Prediction," SAE Technical Paper 780068 (1978), doi:10.4271/780068.
9. Beardsley, M.B., Socie, D., Redja, E., and Berndt, C., "Thick Thermal Barrier Coatings (TTBCs) for Low Emission, High Efficiency Diesel Engine Components," tech. rep., Caterpillar Inc., Peoria, IL, 2006.
10. Beardsley, M.B., *Potential Use of Quasicrystalline Materials as Thermal Barrier Coatings for Diesel Engine Components* (Iowa State University, 2008)
11. Yonushonis, T.M., "Thick Thermal Barrier Coatings for Diesel Components," *NASA Lewis Research Center* (1991).
12. Saad, D., Saad, P., Kamo, L., Mekari, M. et al., "Thermal Barrier Coatings for High Output Turbocharged Diesel Engine," SAE Technical Paper 2007-01-1442 (2007), doi:10.4271/2007-01-1442.
13. Uchida, N. and Osada, H., "A New Piston Insulation Concept for Heavy-Duty Diesel Engines to Reduce Heat Loss from the Wall," *SAE International Journal of Engines* 10, no. 5 (2017): 2565-2574.
14. Schaedler, T., Andruskiewicz, P., Durrett, R., Najt, P. et al., "Temperature-Following Thermal Barrier Coatings for High Efficiency Engines," *DOE Vehicle Technologies Annual Merit Review* (2018).
15. Thibblin, A. and Olofsson, U., "A Study of Suspension Plasma-Sprayed Insulated Pistons Evaluated in a Heavy-Duty Diesel Engine," *International Journal of Engine Research* 21, no. 6 (2020): 987-997.
16. Yan, Z., Gainey, B., Gohn, J., Hariharan, D. et al., "The Effects of Thick Thermal Barrier Coatings on Low-Temperature Combustion," *SAE International Journal of Advances and Current Practices in Mobility* 2, no. 2020-01-0275 (2020): 1786-1799.
17. Morel, T., Keribar, R., and Blumberg, P.N., "Cyclical Thermal Phenomena in Engine Combustion Chamber Surfaces," SAE Technical Paper 850360 (1985), doi:10.4271/850360.
18. Assanis, D.N. and Heywood, J.B., "Development and Use of a Computer Simulation of the Turbocompounded Diesel System for Engine Performance and Component Heat Transfer Studies," 1986.
19. Kamo, R., Assanis, D.N., and Bryzik, W., "Thin Thermal Barrier Coatings for Engines," *SAE Transactions* (1989): 131-136.
20. Wong, V.W., Bauer, W., Kamo, R., Bryzik, W. et al., "Assessment of Thin Thermal Barrier Coatings for IC Engines," *SAE Transactions* (1995): 1640-1650.
21. Mendera, K.Z., "Effects of Plasma Sprayed Zirconia Coatings on Diesel Engine Heat Release," *Journal of KONES* 7, no. 1-2 (2000): 382-389.
22. Hejwowski, T. and Weroński, A., "The Effect of Thermal Barrier Coatings on Diesel Engine Performance," *Vacuum* 65, no. 3-4 (2002): 427-432.
23. Tree, D.R., Wiczynski, P.D., and Yonushonis, T.M., "Experimental Results on the Effect of Piston Surface Roughness and Porosity on Diesel Engine Combustion," *SAE Transactions* (1996): 112-121.
24. Kosaka, H., Wakisaka, Y., Nomura, Y., Hotta, Y. et al., "Concept of "Temperature Swing Heat Insulation" in Combustion Chamber Walls, and Appropriate Thermo-Physical Properties for Heat Insulation Coat," *SAE International Journal of Engines* 6, no. 1 (2013): 142-149.
25. Wakisaka, Y., Inayoshi, M., Fukui, K., Kosaka, H. et al., "Reduction of Heat Loss and Improvement of Thermal Efficiency by Application of "Temperature Swing" Insulation to Direct-Injection Diesel Engines," *SAE International Journal of Engines* 9, no. 3 (2016): 1449-1459.
26. Koutsakis, G. and Ghandhi, J., "Analytical Solution of Unsteady Heat Conduction in Multilayer Internal Combustion Engine Walls," *Applied Thermal Engineering*, 2022 (Under Review).
27. Koutsakis, G., Nellis, G.F., and Ghandhi, J.B., "Surface Temperature of a Multi-Layer Thermal Barrier Coated Wall Subject to an Unsteady Heat Flux," *International Journal of Heat and Mass Transfer* 155 (2020).
28. Koutsakis, G. and Ghandhi, J.B., "An Analytical Approach for Calculating Instantaneous Multilayer-Coated Wall Surface Temperature in an Engine," *SAE International Journal of Advances and Current Practices in Mobility* 2 (2020): 1303-1313.
29. Ghandhi, J. and Koutsakis, G., "Comment on "Numerical Approach to Define a Thermodynamically Equivalent Material for the Conjugate Heat Transfer Simulation of Very Thin Coating Layers" by P. Olmeda, X. Margot, P. Quintero, J. Escalona, International Journal of Heat and Mass Transfer,

Vol. 162 (2020) 120377," *International Journal of Heat and Mass Transfer* 173 (2021): 121190.

30. Babu, A., Koutsakis, G., Kokjohn, S., and Andrie, M., "Experimental and Analytical Study of Temperature Swing Piston Coatings in a Medium-Duty Diesel Engine," SAE Technical Paper 2022-01-0442 (2022), doi:10.4271/2022-01-0442.
31. Koutsakis, G., Miles, S., and Ghandhi, J., "Assessment of In-Cylinder Thermal Barrier Coatings over a Full Vehicle Drive Cycle, SAE Technical Paper 2021-01-0456," (2021), doi:10.4271/2021-01-0456.
32. Koutsakis, G. and Ghandhi, J.B., "Optimization of Thermal Barrier Coating Performance and Durability over a Drive Cycle," *International Journal of Engine Research* (2022).
33. Saputo, J.C., Smith, G.M., Lee, H., Sampath, S. et al., "Thermal Swing Evaluation of Thermal Barrier Coatings for Diesel Engines," *Journal of Thermal Spray Technology* (2021): 1-15.
34. Chérel, J., Zaccardi, J.-M., Bouteiller, B., and Allimant, A., "Experimental Assessment of New Insulation Coatings for Lean Burn Spark-Ignited Engines," *Oil & Gas Science and Technology-Revue d'IFP Energies Nouvelles* 75 (2020): 11.
35. Andrie, M., Kokjohn, S., Paliwal, S., Kamo, L.S. et al., "Low Heat Capacitance Thermal Barrier Coatings for Internal Combustion Engines," SAE Technical Paper 2019-01-0228 1 (2019): 1-13, doi:10.4271/2019-01-0228.
36. de Goes, W.U., Somhorst, J., Markocsan, N., Gupta, M. et al., "Suspension Plasma-Sprayed Thermal Barrier Coatings for Light-Duty Diesel Engines," *Journal of Thermal Spray Technology*, vol. 28, no. 7, pp. 1674-1687, 2019.
37. Somhorst, J., Oevermann, M., Bovo, M., and Denbratt, I., "Evaluation of Thermal Barrier Coatings and Surface Roughness in a Single-Cylinder Light-Duty Diesel Engine," *International Journal of Engine Research* (2019).
38. Thibblin, A., Kianzad, S., Jonsson, S., and Olofsson, U., "Running-In Behaviour of Thermal Barrier Coatings in the Combustion Chamber of a Diesel Engine," *Proceedings of the Institution of Mechanical Engineers, Part D: Journal of Automobile Engineering* (2019).
39. Uchida, N., "A Novel Technology Assessment Chart for Thermal Efficiency Improvement of IC Engines," *International Journal of Engine Research* (2021): 14680874211009671.
40. Koutsakis, G., Begley, M.R., Hutchinson, J.W., and Ghandhi, J.B., "Transient Thermo-Mechanical Analysis of Reciprocating Engine Thermal Barrier Coatings," *Journal of Surface and Coatings Technology* (2022).
41. Gingrich, E., Tess, M., Korivi, V., and Ghandhi, J., "High-Output Diesel Engine Heat Transfer: Part 1 - Comparison between Piston Heat Flux and Global Energy Balance," *International Journal of Engine Research* (2021).
42. Gingrich, E., Tess, M., Korivi, V., Schihl, P. et al., "The Impact of Piston Thermal Barrier Coating Roughness on High-Load Diesel Operation," *International Journal of Engine Research* (2019).
43. Overbye, V.D., Bennethum, J.E., Uyehara, O., and Myers, P., "Unsteady Heat Transfer in Engines," *SAE Transactions* 69 (1961): 461-494.
44. Chang, J., G¨uralp, O., Filipi, Z., Assanis, D. et al., "New Heat Transfer Correlation for an HCCI Engine Derived from Measurements of Instantaneous Surface Heat Flux," *SAE Transactions* (2004): 1576-1593.
45. Gingrich, E., "High-Output Diesel Engine Heat Transfer," PhD Thesis, University of Wisconsin-Madison, 2020.
46. Srinivasan, V., Friis, M., Vaidya, A., Streibl, T. et al., "Particle Injection in Direct Current Air Plasma Spray: Salient Observations and Optimization Strategies," *Plasma Chemistry and Plasma Processing* 27, no. 5 (2007): 609-623.
47. ASTM, "E1461-01," *Standard Test Method for Thermal Diffusivity by the Flash Method*, 2001.
48. Nakamura, T. and Liu, Y., "Determination of Nonlinear Properties of Thermal Sprayed Ceramic Coatings via Inverse Analysis," *International Journal of Solids and Structures* 44, no. 6 (2007): 1990-2009.
49. Liu, Y., Nakamura, T., Dwivedi, G., Valarezo, A. et al., "Anelastic Behavior of Plasma-Sprayed Zirconia Coatings," *Journal of the American Ceramic Society* 91, no. 12 (2008): 4036-4043.
50. Dwivedi, G., Nakamura, T., and Sampath, S., "Controlled Introduction of Anelasticity in Plasma-Sprayed Ceramics," *Journal of the American Ceramic Society* 94 (2011): s104-s111.
51. Tan, Y., Shyam, A., Choi, W.B., Lara-Curzio, E. et al., "Anisotropic Elastic Properties of Thermal Spray Coatings Determined via Resonant Ultrasound Spectroscopy," *Acta Materialia* 58, no. 16 (2010): 5305-5315.
52. Smith, G.M., Resnick, M., Kjellman, B., Wigren, J. et al., "Orientation-Dependent Mechanical and Thermal Properties of Plasma-Sprayed Ceramics," *Journal of the American Ceramic Society* 101, no. 6 (2018): 2471-2481.
53. Tsui, Y.a.-C. and Clyne, T., "An Analytical Model for Predicting Residual Stresses in Progressively Deposited Coatings Part 1: Planar Geometry," *Thin Solid Films* 306, no. 1 (1997): 23-33.
54. Matejicek, J., Sampath, S., Brand, P., and Prask, H., "Quenching, Thermal and Residual Stress in Plasma Sprayed Deposits: NiCrAlY and YSZ Coatings," *Acta Materialia* 47, no. 2 (1999): 607-617.
55. Chandra, L. and Clyne, T., "Possible Technique for the Characterization of Diamond Films using an Ultrasonic Resonance Technique," *Diamond and Related Materials* 2, no. 5-7 (1993): 977-983.
56. Slim, M.F., Alhussein, A., Billard, A., Sanchette, F. et al., "On the Determination of Young's Modulus of Thin Films with Impulse Excitation Technique," *Journal of Materials Research* 32, no. 3 (2017): 497-511.
57. Paul, S., "Stiffness of Plasma Sprayed Thermal Barrier Coatings," *Coatings* 7, no. 5 (2017): 68.
58. ASTM, "E1820-01," *Standard Test Method for Measurement of Fracture Toughness*, 2001.
59. Smith, G.M., Smith, A., and Sampath, S., "Fracture Toughness of Thermal Spray Ceramics: Measurement Techniques and Processing Dependence," *Journal of Thermal Spray Technology* 27, no. 7 (2018): 1076-1089.
60. Donohue, E.M., *Investigation of the Parameters Influencing Thermal Barrier Coating Toughness Through a Novel*

Measurement Technique. University of California, Santa Barbara, 2014.

61. Hendricks, T.L., "Instantaneous Heat Flux Measurements in Internal Combustion Engines," PhD Thesis, University of Wisconsin-Madison, 2011.
62. Sundaram, S., Lipkin, D., Johnson, C., and Hutchinson, J.W., "The Influence of Transient Thermal Gradients and Substrate Constraint on Delamination of Thermal Barrier Coatings," *Journal of Applied Mechanics* 80, no. 1 (2013).

Contact Information

G. Koutsakis
Engine Research Center
University of Wisconsin-Madison
koutsakis@wisc.edu

Acknowledgments

This work was completed utilizing Army in-house laboratory independent research (ILIR) basic research funds in coordination with the Office of Naval Research grant N00014-16-1-3036 to Stony Brook University.

Support for this work was provided by Deere & Company to University of Wisconsin-Madison.

Definitions, Acronyms, Abbreviations

Nomenclature

k - Thermal Conductivity [$Wm^{-1}K^{-1}$]

ρ - Density [kgm^{-3}]

c - Specific heat capacity [$Jkg^{-1}K^{-1}$]

L - Length [m]

α - Coefficient of Thermal Expansion [K^{-1}]

ν - Poisson Ratio [-]

E - Young's Modulus [GPa]

x - Position x [m]

y - Position y [m]

U - Strain energy [Jm^{-2}]

K_{IC} - Fracture toughness or Critical Stress Intensity Factor [MPa $\sqrt{m}$]

G - Energy Release Rate [kJm^{-2}]

G_c - Toughness [kJm^{-2}]

Abbreviations

TBC - Thermal Barrier Coating

FGM - Functionally Graded Material

SOI - Start of Injection

FFT - Fast Fourier Transform

(a)TDC - (after) Top Dead Center

BDC - Bottom Dead Center

IMEPg - Gross Indicated Mean Effective Pressure

YSZ - Yttria Stabilized Zirconia

APS - Atmospheric Plasma Spray

CTE - Coefficient of Thermal Expansion

SENB - Single Edge Notch Bend

AHRR - Apparent Heat Release Rate

Appendix

TABLE 4 Summary of atmospheric plasma spray characteristics

Coating	Ar	H_2	Current	Carrier Gas	Stress-Free Temperature
	[NLMP]	[bar]	[A]	[NLMP]	[°C]
Bond Coat	46	6	550	2.5	220
YSZ Thin/Thick	35	8	450	4	220
Cordierite-YSZ Compliant	45	6	550	3	240
Cordierite-YSZ Stiff	45	6	550	3	240

TABLE 5 Thermo-mechanical properties of wall architectures investigated, with k: thermal conductivity, ρ: density, c: specific heat capacity, L: thickness, E: Young's modulus α: coefficient of thermal expansion, ν: Poisson ratio, t_{ref}: stress-free temperature and G_c: toughness

Wall Structure	Layer	Material	k [W/m-K]	ρ [kg/m^3]	c [J/kg-K]	L [μm]	E [GPa]	α [ppm K^{-1}]	ν [-]	t_{ref} [°C]	G_c [J/m^2]
Four-layer YSZ[42]	Top	8YSZ	0.77	4713	387	195	41	11.7	0.17	220	95±22
	Gradient	mix	0.85	3886	385	65	50	14.5	0.17	220	150
	Bond	443NS	4.07	6255	152	65	55	16.4	0.2	220	436
	Piston	4140	39	7850	520	4675	180	13.5	0.29	—	—
Thin	Top	8YSZ	0.89	5586	387	275	30	11.5	0.17	220	113±20
	Bond	443NS	4.85	7120	395.2	50	55	16.4	0.2	220	436
	Piston	4140 Steel	39	7850	520	4675	180	13.5	0.29	—	—
Thick	Top	8YSZ	0.89	5586	387	470	30	11.5	0.17	220	113±20
	Bond	443NS	4.85	7120	395.2	50	55	16.4	0.2	220	436
	Piston	4140 Steel	39	7850	520	4480	180	13.5	0.29	30	—
Compliant	Top	Cordierite	0.39	2894	347.4	275	15	7	0.17	240	53±11
	Bond	443NS	4.85	7120	395.2	50	55	16.4	0.2	240	436
	Piston	4140 Steel	39	7850	520	4675	180	13.5	0.29	—	—
Stiff	Top	Cordierite	0.89	3619	579	275	46.9	7.5	0.17	240	28±6
	Bond	443NS	4.85	7120	395.2	50	55	16.4	0.2	240	436
	Piston	4140 Steel	39	7850	520	4675	180	13.5	0.29	—	—

ISSN 0148-7191